Sol–gel synthesis and sintering of submicronic copper molybdate (α-CuMoO4) powders

Mohamed Benchikhi, Rachida El Ouatib, Sophie Guillemet-Fritsch, Jean-Yves Chane-Ching, Lahcen Er-Rakho, Bernard Durand

Sol–gel synthesis and sintering of submicronic copper molybdate (α-$CuMoO_4$) powders

Mohamed Benchikhi[a,b], Rachida El Ouatib[a], Sophie Guillemet-Fritsch[b], Jean Yves Chane-Ching[b], Lahcen Er-Rakho[a], Bernard Durand[b,*]

[a]*Laboratoire de Physico-Chimie des Matériaux Inorganiques, Université Hassan II, Casablanca, Morocco*
[b]*Institut Carnot CIRIMAT, Université de Toulouse, CNRS, 118 Route de Narbonne, 31062 Toulouse Cedex 9, France*

Abstract

A sol–gel method was proposed to prepare copper II molybdate α-$CuMoO_4$ powders. A gel was first obtained via the polymerizable complex method, using citric acid as complexing and polymerizing agent, dried at 120 °C and decomposed at 300 °C. A calcination in the temperature range 400–500 °C for 2 h led to the pure phase α-$CuMoO_4$. The different powders obtained were characterized by X ray diffraction analysis and by transmission (TEM) and scanning (SEM) electron microscopies.

Ceramics were prepared using conventional sintering and spark plasma sintering (SPS) techniques. A maximal relative density of 94.8% was reached after conventional sintering at 520 °C for 2 h. In the case of SPS, the densification was optimized by varying the temperature, the time and the applied pressure. Higher densities, up to 98.7%, were obtained at very low temperature, i.e., 300 °C, for 5 min only under a pressure of 225 MPa.

Keywords: A. Sintering; B. Grain size; Sol–gel; Powders; Chemical preparation

1. Introduction

Copper molybdate $CuMoO_4$ exhibits two polymorphs at atmospheric pressure, the α form with Mo located in a tetrahedral environment (stable form) and the γ form with Mo located in an octahedral environment (metastable form). This oxide appears as a true horn of numerous note-worthy properties: it is thermochromic, trisochromic and piezochromic since it exhibits a phase transition associated with a color change from green to brown. This first order transition is accompanied by a strong change of volume and an anisotropic splitting of grains and occurs according to a domino-cascade kinetics. Moreover, the temperatures/pressures of transition are adjustable by chemical doping. So, copper molybdate $CuMoO_4$ can find applications as catalyst, pressure and/or temperature sensor. The complexity of $CuMoO_4$ justifies the numerous studies on this oxide [1–5].

Several methods of copper molybdate preparation have been investigated, particularly those involving solid state reactions between copper and molybdenum oxides at temperatures close to 750 °C [6,7] and those involving pyrolysis at about 500 °C of precursors precipitated at low temperature [8] or obtained by sol–gel [9].

This paper deals with the synthesis of a homogenous and finely divided powder of α-$CuMoO_4$ and the elaboration of the corresponding dense ceramics using spark plasma sintering.

The route involving the polymerizable complex, based on the Pechini method [10], was chosen. It leads to sub-micronic sized particles and also offers the advantage to increase the reactivity of reaction mixtures. The final powders synthetized this way usually present high homogeneity [11].

2. Experimental

The gels were synthesized using the following reactants: ammonium heptamolybdate $(NH_4)_6Mo_7O_{24}\cdot 4H_2O$ (Sigma-Aldrich

*Corresponding author. Tel.: +33 56 1557751; fax: +33 56 1556163.
E-mail address: bdurand@chimie.ups-tlse.fr (B. Durand).

http://dx.doi.org/10.1016/j.ceramint.2013.10.118

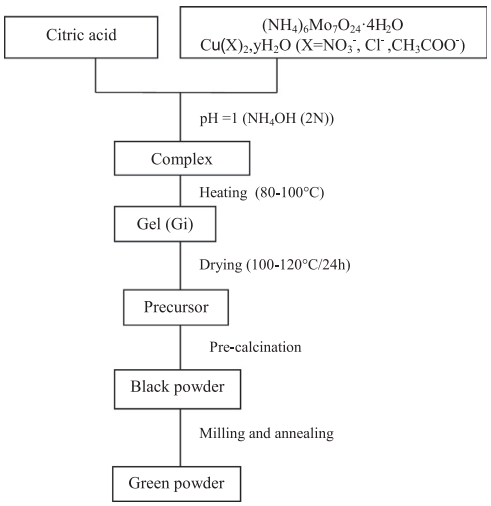

Fig. 1. Flowchart of the synthesis of $CuMoO_4$ by the polymerizable complex method.

99%), copper salts CuX_2–nH_2O (X=NO_3^-) (Acros Organics 99.5%), Cl^- (Acros Organics 99.5%), CH_3COO^- (Fluka 99.8%), citric acid (Acros 99.5%), concentrated nitric acid and ammonia.

The procedure for copper molybdate synthesis from a polymeric precursor is shown in Fig. 1. A citric acid (CA) solution was added to an equimolar solution of ammonium molybdate and copper salt in a proportion such that CA/cation=3; the pH was close to pH1. The evaporation of the solution at 80 °C led to the formation of gels named Gi (*i* is the source of copper; *i*=1 nitrate, *i*=2 chloride, and *i*=3 acetate). The gels were dried at 120 °C for 24 h, then pre-calcined at 300 °C for 12 h.

The black powders obtained were treated under air at temperature ranging from 420 to 500 °C according to the nature of the copper source. The final calcination temperatures could be optimized after thermogravimetry analyses (SETERAM TG-DTA 92). The green powders obtained at the end of the process were characterized by X-ray diffraction (Brucker AXSD4, λCuKα=1.5418 nm), by scanning (Jeol-JSM6400) and transmission (Jeol 2010) electron microscopies. Specific surface areas were determined using a BET (Micrometrics Flowsorb II 2300). The precise chemical compositions were obtained by ICP-AES (JobinYvon ULTIMA). The sintering behavior was studied by dilatometry (TMA Setsys 16/18). The ceramics were obtained using both conventional sintering in air performed in a muffle furnace (Nabertherm) and by spark plasma sintering (SPS 2080, Sumitomo).

3. Results and discussion

3.1. Powders

The nature of the copper precursor (nitrate, chloride or acetate) had only a very weak influence on the properties of the gels obtained. Indeed, according to the ICP analysis data (Table 1), the Cu/Mo molar ratio in different gels was close to 1, whatever the copper source. Moreover, the thermogravimetric curves of the dried gels, performed in air at a rate of 2.5 °C/min were very similar (Fig. 2) and revealed several decomposition steps (Table 2) with a total mass loss always close to 65%. The main difference was noticed for the temperature of the end of decomposition which increased following the sequence chloride (385 °C), nitrate (420 °C) and copper acetate (440 °C). The faster decomposition of the gel G_2 was corroborated by the X-ray diffraction analyses of the gel powders calcined at different temperatures (Fig. 3). In the patterns of gels calcined at 300 °C for 12 h, mixtures of three phases were identified: α-$CuMoO_4$ (JCPDS 073-0488), MoO_3

Table 1
ICP analysis of $CuMoO_4$ powders obtained from gels Gi.

Gel	Cu (wt%)	Mo (wt%)	Cu/Mo (molar ratio)
G1	28.4	42.6	1.01
G2	27.9	41.1	1.03
G3	27.8	41.6	1.01

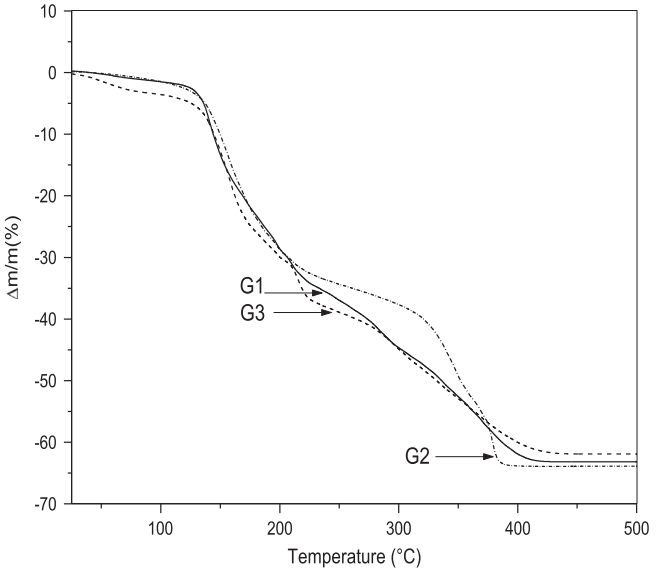

Fig. 2. Thermogravimetric analysis of the xerogels Gi (G1 nitrate, G2 chloride, and G3 acetate).

Table 2
Temperature and mass loss of the different phenomena determined by TGA for the gels Gi.

Gel	Temperature range (°C)	Mass loss (%)
G1	25–125	2.5
G1	125–226	31.8
G1	226–420	28.7
G2	25–100	1.1
G2	100–235	32.0
G2	226–385	24.5
G3	25–120	9.5
G3	120–190	29.3
G3	231–440	24.7

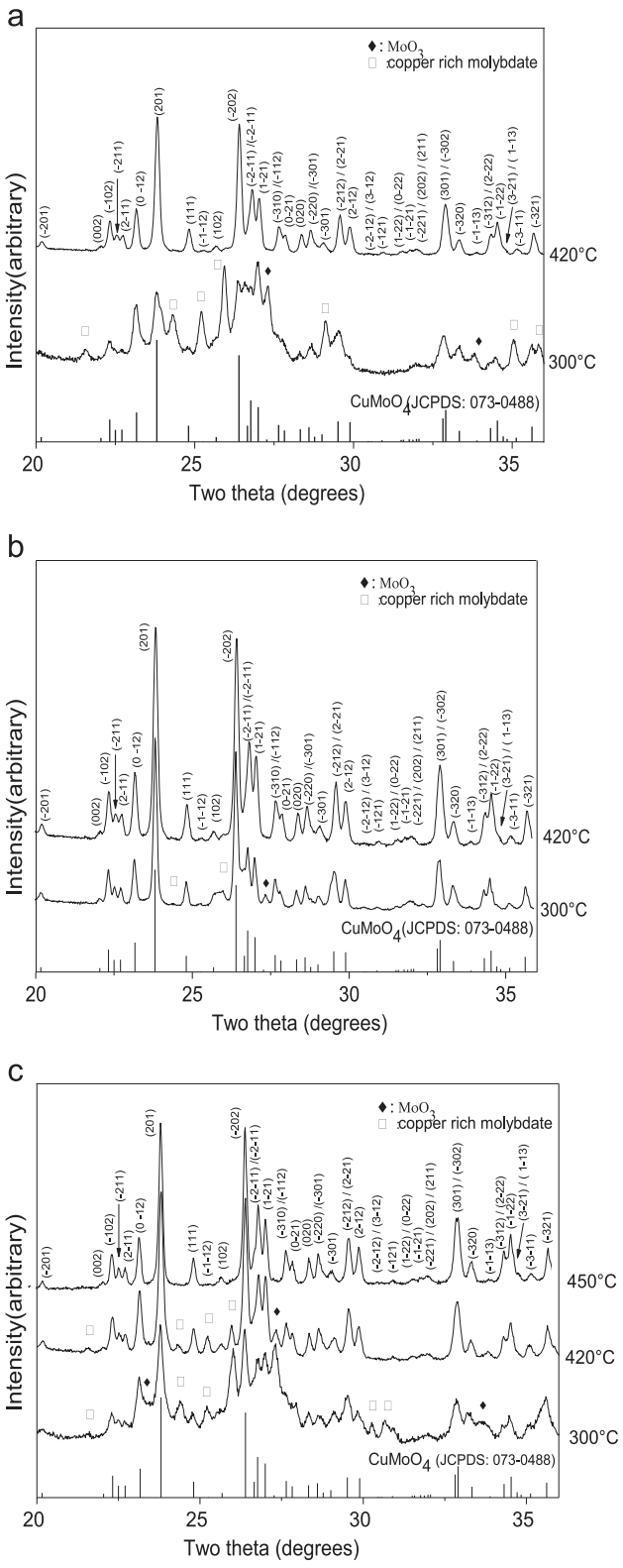

Fig. 3. XRD patterns of gels Gi treated at different temperatures: (a) G1 treated at 300 and 420 °C, (b) G2 treated at 300 and 420 °C, and (c) G3 treated at 300, 420 and 450 °C.

(JCPDS 076-1003) and a phase that should be a mixed oxide of copper and molybdenum richer in copper than $CuMoO_4$. The phase α-$CuMoO_4$ was preponderant and the rays of the additional phases were very weak only when the copper source was the chloride. For gels ex chloride or nitrate, the phase α-$CuMoO_4$ was only identified in the powders calcined at 420 °C for 2 h. For the

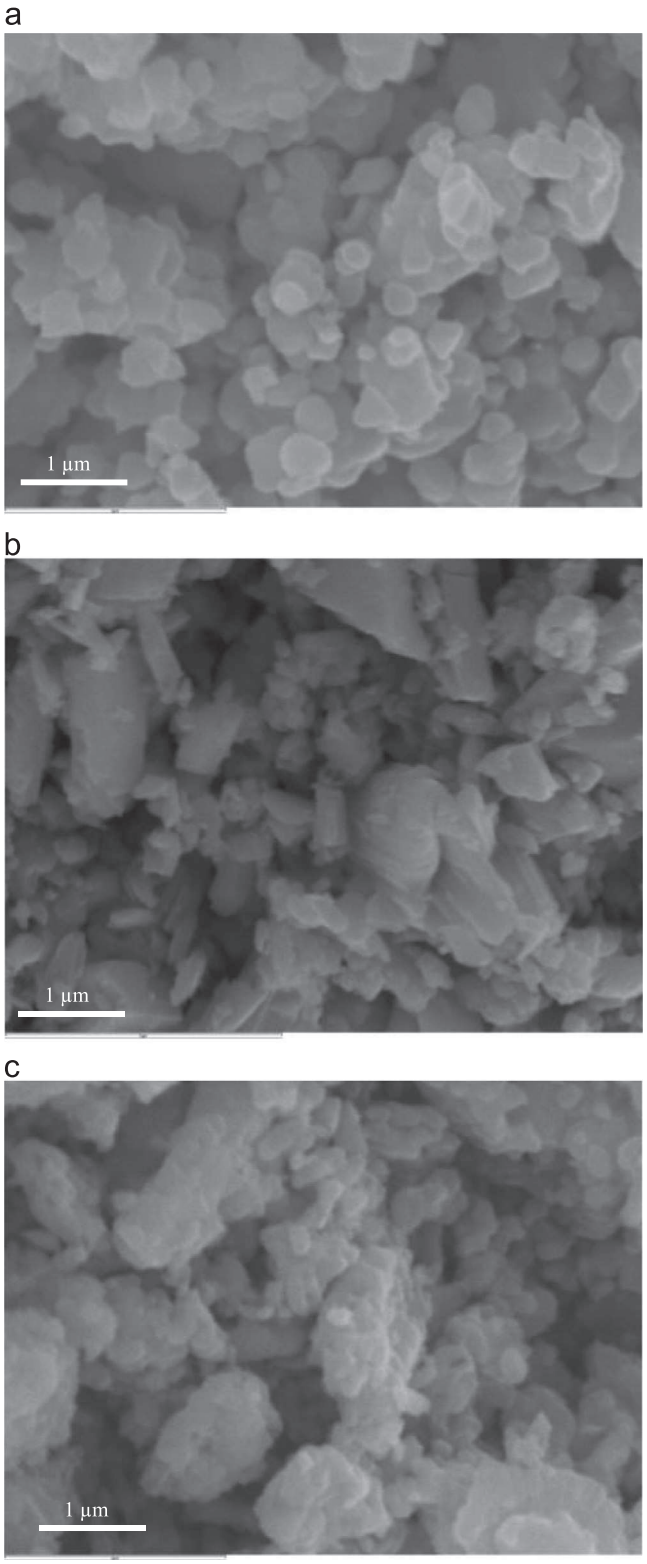

Fig. 4. SEM micrographs of gels Gi synthesized with a CA/Cu ratio = 3: (a) gel G1, (b) gel G2, and (c) gel G3.

Table 3
Sizes estimated by different methods of particles of copper molybdate powders obtained by pyrolysis of gels Gi synthesized with a molar ratio CA/Cu = 3.

Gel	Crystallite size DRX[a] (nm)	S_{BET} (m^2/g)	Grain size BET[b] (nm)	Grain size TEM[c] (nm)
G1	103	8.3	168	100–200
G2	138	6.9	202	140–250
G3	145	6.8	206	150–280

[a]Size of crystallites calculated from XRD peaks broadening.
[b]Geometrical size of particles calculated from the specific surface area.
[c]Size of particles estimated by TEM.

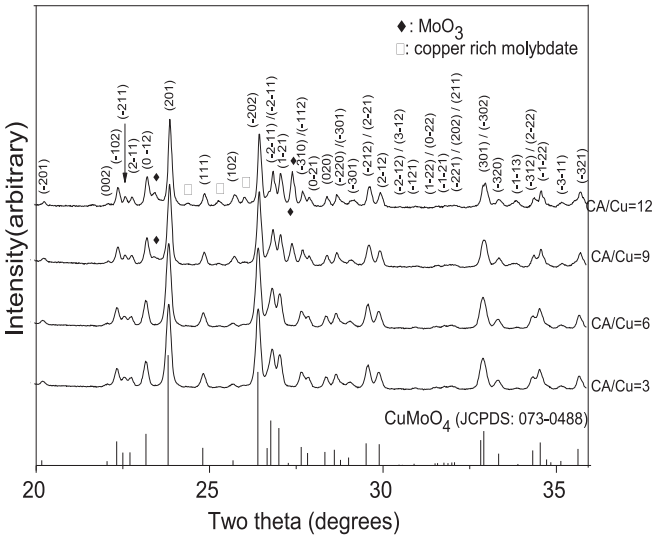

Fig. 5. XRD patterns of gel nitrate (G1) treated at 420 °C for 2 h for different CA/Cu ratios.

gel ex acetate, the calcination temperature had to be raised up to 450 °C to obtain the same result.

The α-$CuMoO_4$ powders, obtained by calcination for 2 h of gels G1 and G2 at 420 °C and G3 at 450 °C, consisted in elongated or more or less spherical elementary grains with sizes in the range 0.2–1.0 μm (Fig. 4). The crystallite sizes (calculated according to the Scherrer equation from the broadening of X-ray diffraction peaks), the geometrical sizes of particles (calculated from the experimental values of specific surface area assuming that powders are made of monodispersed spherical grains) and the sizes of grains measured on TEM micrographs (Fig. 6a for G1) were of the same order of magnitude (Table 3). TEM observations could evidence some monocrystalline particles.

The influence of the CA/Cu molar ratio on the morphology of powders was examined. The ratio was varied between 3 and 12. The XRD patterns of the molybdates formed by calcination of the gels at 420 or 450 °C for 2 h showed that whatever the source of copper, beyond a molar ratio of 6, molybdenum oxide MoO_3 was formed beside α-$CuMoO_4$ (as shown in Fig. 5 for gel G1). TEM micrographs revealed that increasing the ratio from 3 to 6 significantly raised crystallite size (Fig. 6).

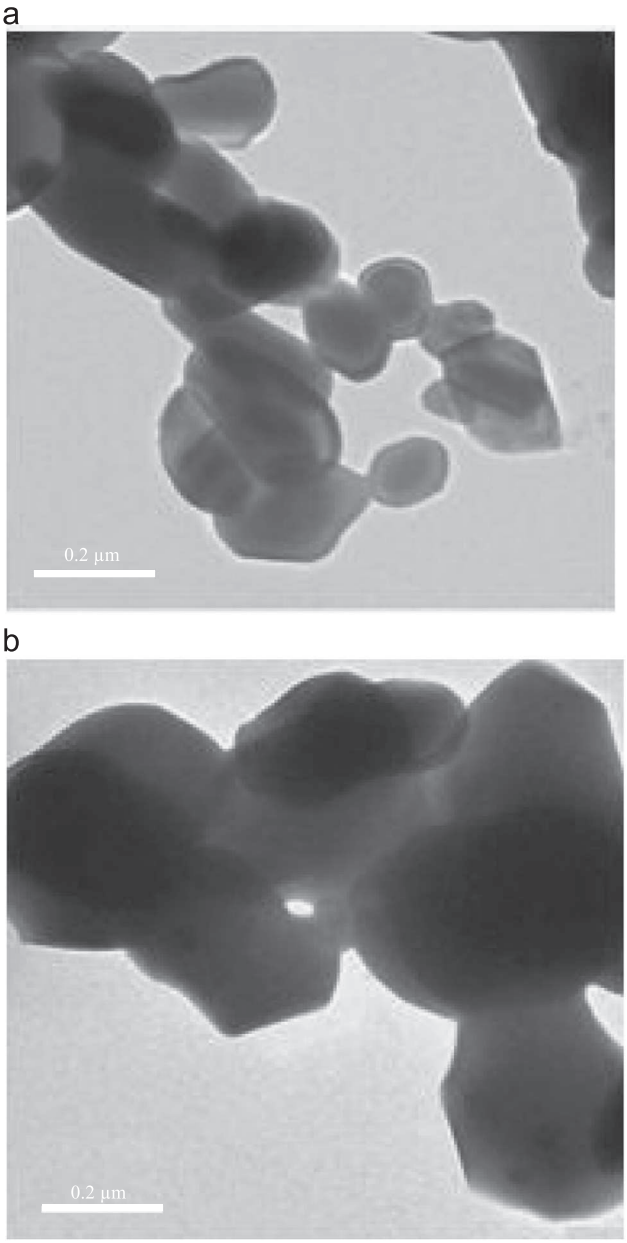

Fig. 6. TEM micrographs of gel nitrate (G1) treated at 420 °C for 2 h for different CA/Cu ratios: (a) CA/Cu = 3, and (b) CA/Cu = 6.

3.2. Bulk ceramics

The sintering behavior was investigated on the α-$CuMoO_4$ powders obtained by pyrolysis at 420 °C for 2 h of a gel prepared from copper chloride with a citrate/copper ratio of 3.

For conventional sintering, discs were formed by uniaxial pressing at 25 bars at room temperature in the presence of an organic binder (Rhodoviol) so as to avoid the phenomenon of rolling. The green density reached 61%. The dilatometric curve recorded at a rate of 2.5 °C/min (Fig. 7) indicated the release of the binder at ~190 °C and the beginning of shrinkage at approximately 430 °C. The shrinking rate was maximum at 520 °C.

Conventional sintering treatments were then performed in air, in a muffle furnace at 520 °C and 570 °C, for 1, 2 and 6 h.

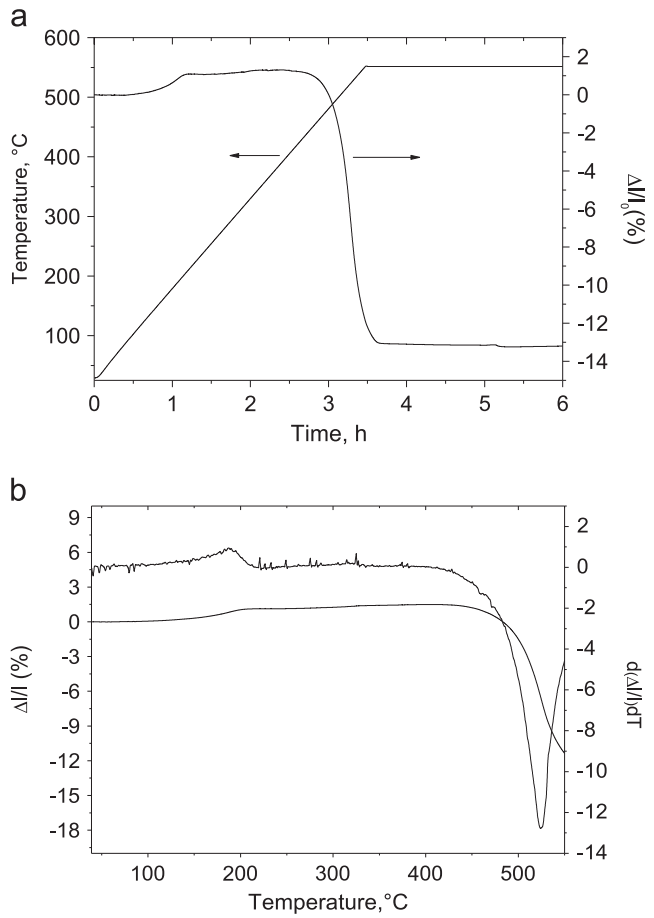

Fig. 7. Dilatometric behavior of $CuMoO_4$: (a) $\Delta l/l$ and temperature versus time, and (b) $\Delta l/l$ and derivate of $\Delta l/l$ versus temperature.

Table 4
Influence of the temperature and the time on the relative density of conventionally sintered $CuMoO_4$ ceramics.

Temperature (°C)	Time (h)	Relative density (%)
520	1	92.7
520	2	94.7
520	6	93.6
570	1	93.8
570	2	93.9
570	6	91.4

The densification of the ceramics is shown in Table 4. The highest value, 94.8%, was reached for 2 h sintering at 520 °C, which confirmed the temperature where the shrinking rate was maximum. Prolonging the dwell time was not necessary to increase densification. Under these conditions (2 h, 520 °C), the ceramics consisted of grains sized less than 2 µm, with a relatively narrow granulometric distribution (Fig. 8a). Little residual porosity was observed. The decrease of density after the dwell time was increased to 6 h was likely due to the abnormal growth of some grains (Fig. 8b). For a higher sintering temperature (570 °C), the abnormal growth was even more pronounced (Fig. 8c).

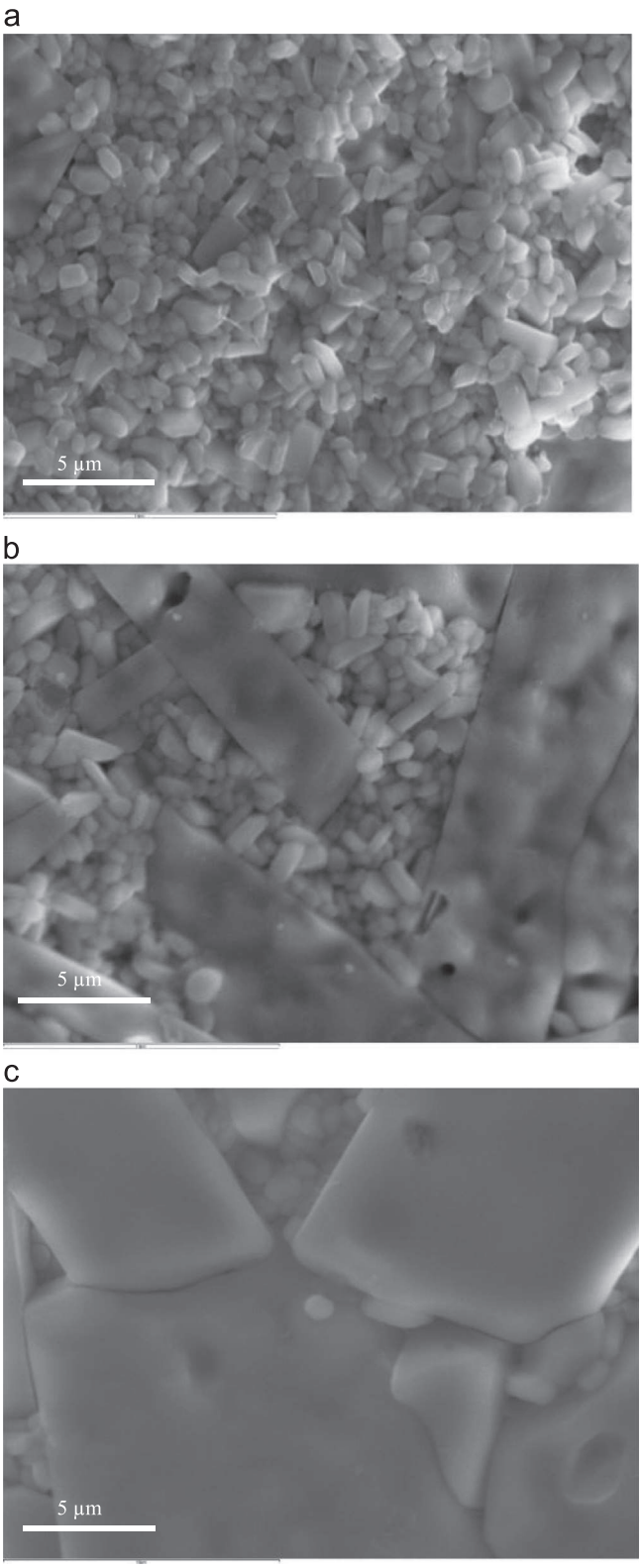

Fig. 8. SEM micrographs of $CuMoO_4$ ceramics conventionally sintered: (a) 520 °C for 2 h, (b) 520 °C for 6 h, and (c) 570 °C for 2 h.

The advantage of the spark plasma sintering technique is to allow sintering at temperatures significantly lower and for times much shorter than those required for natural sintering.

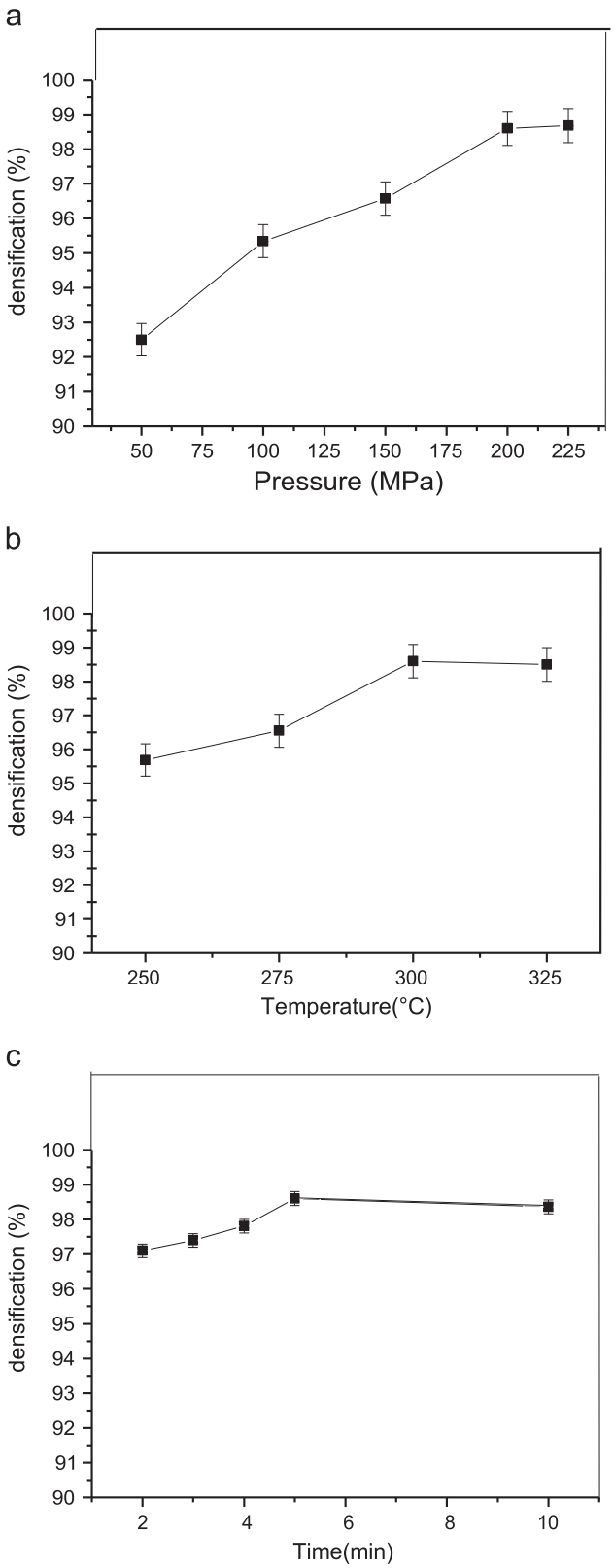

Fig. 9. Densification of SPS sintered $CuMoO_4$ ceramics as a function: (a) the applied pressure, (b) the temperature, and (c) the time.

Different sintering parameters, i.e. the temperature, the dwell time and the applied pressure, were optimized in order to reach the highest densification (Fig. 9, Table 5). A sintering

Table 5
Influence of the temperature, the time and the pressure on the relative density of SPS sintered $CuMoO_4$ ceramics.

Temperature (°C)	Time (min)	Pressure (MPa)	Relative density (%)
300	2	200	97.1
300	5	200	98.6
300	10	200	98.4
275	5	200	96.6
325	5	200	98.5
300	5	175	96.5
300	5	225	98.7
500	2	50	98.5

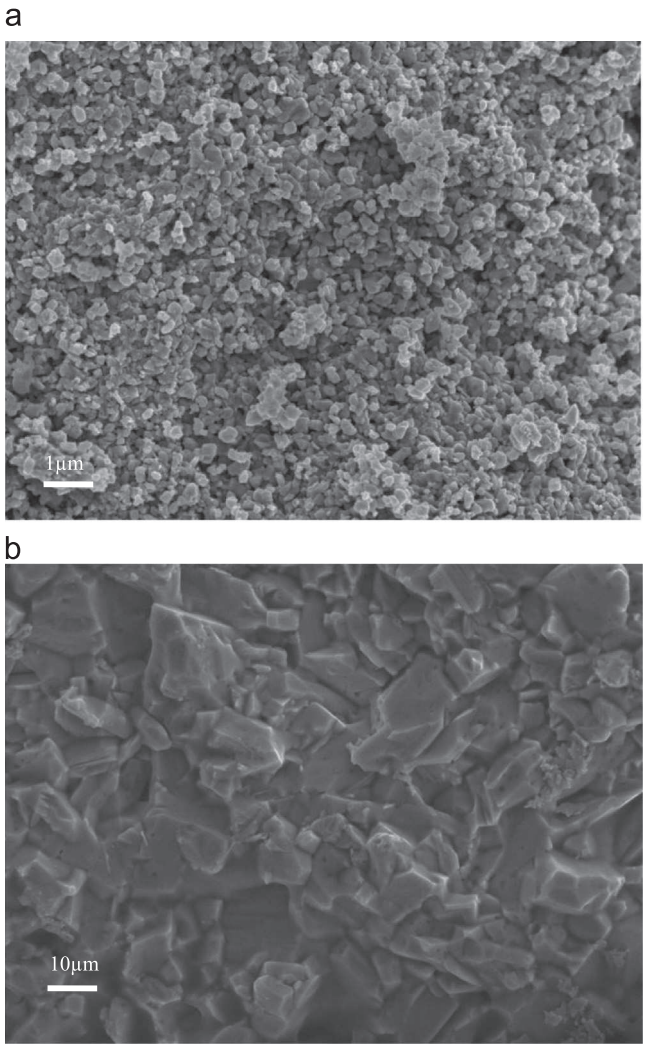

Fig. 10. SEM micrographs of $CuMoO_4$ SPS sintered ceramics: (a) at 300 °C for 2 min with a pressure of 200 MPa, and (b) at 500 °C for 2 min with a pressure of 50 MPa.

temperature of only 300 °C was first arbitrarily chosen. The ceramic showed a relative density of 97.10%, which was indeed higher than the highest value obtained by natural sintering; it was reached with an applied pressure of 200 MPa and a dwell time of 2 min only. A trial at 500 °C

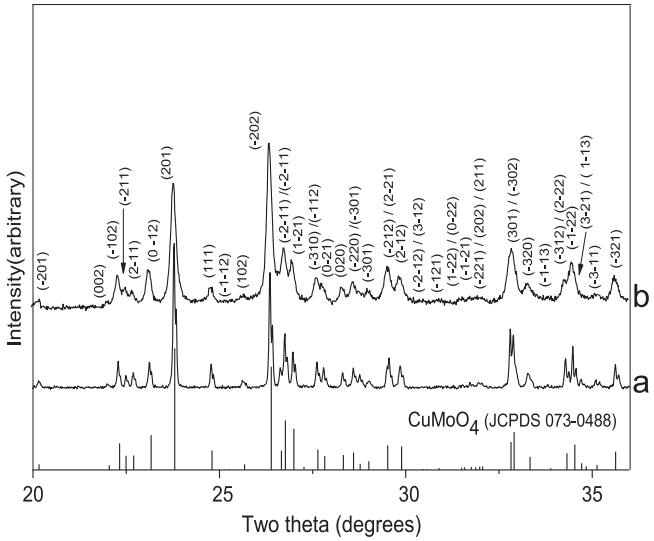

Fig. 11. XRD patterns of $CuMoO_4$: (a) conventionally sintered at 520 °C for 2 h, and (b) SPS sintered at 300 °C for 5 min with an applied pressure of 200 MPa.

under a lower applied pressure so as to avoid the decomposition of the sample did not lead to higher densification. An increase of the level time to 5 min increased the density up to 98.6%. A further increase up to 10 min had no further effect. Taking the basic conditions of temperature and time (300 °C, 2 min), the pressure was also optimized. A maximal density of 98.7% was obtained with a pressure of 225 MPa. As the gain of density obtained when the pressure was increased from 200 to 225 MPa was only very slight, the optimal applied pressure was taken at 200 MPa, which presented less of a risk to break the sample.

The SEM micrographs of ceramics (Fig. 10) revealed that regarding the very short time of sintering and the low temperature of densification, high densities were obtained without significant grain growth. For sintering at 300 °C for 5 min under 200 MPa and at 500 °C for 2 min under 50 MPa, the grain sizes did not exceed respectively 200 nm and 2 μm. The XRD patterns of the ceramics conventionally sintered at 520 °C for 2 h (Fig. 11a) and sintered by SPS at 300 °C for 5 min under 200 MPa (Fig. 11b) showed that, whatever the sintering procedure, the α-$CuMoO_4$ phase is not modified by the thermal treatment. The broadness of the peaks of the SPS sintered ceramic was comparable to that of the peaks of the non-sintered powder (Fig. 3b; 420 °C) whereas the peaks of the conventionally sintered ceramic were significantly narrower. The data of microscopy (Figs. 8 and 10) are confirmed, i.e. on the contrary of conventional route, the SPS allows the limitation of the grain growth.

4. Conclusion

α-$CuMoO_4$ submicronic powders were prepared using a method derived from the Pechini method. Different gels, using various copper salts, i.e. nitrates, chlorides and acetates, were obtained. After calcinations at temperatures ranging from 420 °C to 490 °C, pure α-$CuMoO_4$ phases could be obtained. The grain size was in the range 200–1000 nm.

Spark Plasma Sintering performed at temperatures as low as 300 °C for 5 min only allowed to prepare dense ceramics with the same grain size as the powders.

Acknowledgments

This work was supported by two French-Moroccan projects: Volubilis Partenariat Hubert Curien (PHC n° MA 09 205) and Projet de Recherches sur Convention Internationale CNRS-CNRST n° 22572.

References

[1] F. Rodríguez, D. Hernández, J. Garcia-Jaca, H. Ehrenberg, H. Weitzel, Optical study of the piezochromic transition in $CuMoO_4$ by pressure spectroscopy, Phys. Rev. B 61 (2000) 16497.
[2] M. Gaudon, P. Deniard, A. Demourgues, A.E. Thiry, C. Carbonera, A. Le Nestour, A. Largeteau, J.F. Létard, S. Jobic, Unprecedented "One-Finger-Push"-induced phase transition with a drastic color change in an inorganic material, Adv. Mater. 19 (21) (2007) 3517.
[3] A.E Thiry, M. Gaudon, C. Payen, N. Daro, J.F. Létard, S. Gorsse, P. Deniard, X. Rocquefelte, A. Demourgues, M.H. Whangbo, S. Jobic, On the cyclability of the thermochromism in $CuMoO_4$ and its tungsten derivatives $CuMo_{1-x}W_xO_4$ ($x < 0.12$), Chem. Mater. 20 (6) (2008) 2075.
[4] M. Gaudon, C. Carbonera, A.E. Thiry, A. Demourgues, P. Deniard, C. Payen, J.F. Létard, S. Jobic, Adaptable thermochromism in the $CuMo_{1-x}W_xO_4$ series ($0 < x < 0.1$): a behavior related to a first-order phase transition with a transition temperature depending on x, Inorg. Chem. 46 (24) (2007) 10200.
[5] H. Ehrenberg, H. Weitzel, H. Paulus, M. Wiesmann, G. Wltschek, M. Geselle, H. Fuess, Crystal structure and magnetic properties of $CuMoO_4$ at low temperature (γ-phase), J. Phys. Chem. Solids 58 (1997) 153.
[6] M. Wiesmann, H. Ehrenberg, G. Miehe, T. Peun, H. Weitzel, H. Fuess, p-TPhase diagram of $CuMoO_4$, J. Solid State Chem. 132 (1) (1997) 88.
[7] D. Klissurski, R. Iordanova, M. Milanova, D. Radev, S. Vassilev, Mechanochemically assisted synthesis of Cu (II) molybdate, CR Acad. Bulgare Sci. 56 (8) (2003) 39.
[8] S. Mitchell, A. Gómez-Avilés, C. Gardner, W. Jones, Comparative study of the synthesis of layered transition metal molybdates, J. Solid State Chem. 183 (1) (2010) 198.
[9] J.H. Ryu, S-M Koo, J-W Yoon, C.S. Lim, K.B. Shim, Synthesis of nanocrystalline $MMoO_4$ (M=Ni, Zn) phosphors via a citrate complex route assisted by microwave irradiation and their photoluminescence, Mat. Lett. 60 (13–14) (2006) 1702.
[10] M. Pechini, U.S. Patent 3,330,697, 11 July 1967.
[11] C.N.R. Rao, B. Raveau, Transition Metal Oxides, VCH, New York, 1995.